SUPPLEMENTARY INFORMATION

The SRP-SR co-translational targeting complex in the *closed* state displays flexible NG-domains and a defined M-domain with signal sequence

Ottilie von Loeffelholz[a,b,e,1], Qiyang Jiang[a,b,1], Aileen Ariosa[c], Manikandan Karuppasamy[a,b], Karine Huard[a,b], Imre Berger[a,b,d], Shu-ou Shan[c], and Christiane Schaffitzel[a,b,d,2]

Affiliations:

[a]European Molecular Biology Laboratory, Grenoble Outstation, Grenoble, 38042 France

[b]Unit for Virus Host-Cell Interactions, Univ. Grenoble Alpes-EMBL-CNRS, Grenoble, 38042 France

[c]Division of Chemistry and Chemical Engineering, California Institute of Technology, Pasadena, CA 91125

[d]School of Biochemistry, University of Bristol, Bristol, BS8 1TD, United Kingdom

[e]Current address: Institute of Structural and Molecular Biology, Birkbeck College, London, WC1E 7HX, United Kingdom

[1] These authors contributed equally to this work.

[2]To whom correspondence should be addressed:

Christiane Schaffitzel, EMBL, 71 avenue des Martyrs, CS 90181, 38042 Grenoble Cedex 9, France. Telephone: +33 4 76 20-7505. Email: schaffitzel@embl.fr

SI METHODS

Cloning of scSRP^{219}, scSRP^{219}2 and FtsY^{219}

To generate an expression plasmid for scSRP^{219} the truncated version of FtsY (FtsY^{219}) was amplified by PCR from a plasmid encoding for scSRP (1) with a forward primer containing part of the sequence coding for a Strep-tag II affinity tag (iba lifesciences) and annealing to the FtsY sequence from amino acid 220 on (5'-ccgcagttcgaaaaagccggcagcggcggtaaaaaaatcgacgatgatctg-3') and a reverse primer aligning to the C-terminal end of FtsY with an additional C-terminal *Pst*I restriction site (5'-tctagactgcaggcgtccggctgtatc-3'). The N-terminus of the PCR product was elongated by the remaining StrepII tag sequence via a second PCR another forward primer containing an N-terminal *Nde*I restriction site (5'-tctagacatatggctagctggagccac ccgcagttcgaaaaagccgg-3'). This PCR product digested with *Nde*I and *Pst*I and ligated into the *Nde*I/*Pst*I-digested pET24aFtsYlinkFfh plasmid (1) yielding pET24aFtsYΔNlinkFfh. pET24aFtsYΔNlinkFfh encodes a fusion of residues 220-498 of *E. coli* FtsY and the complete *E. coli* Ffh protein (residues 1-453) linked via a 31 amino acids glycine-serine rich linker.

A second plasmid encodoing scSRP^{219} with an N-teminal hexahistidine-tag and a C-terminal StrepII-tag (scSRP^{219}2) was generated from a PCR product using the pET24aFtsYΔNlinkFfh plasmid by PCR using as a template and (5'-aattaacatatgcatcatcaccatcaccatggtaaaaaa atcgacgatgatc-3' and 5'-attaataagcttagccgctacccgctttctcaaactgcggatggctccatgacgcagatctgcgaccag ggaag-3') as PCR primers. The PCR product was fused into pET24a by *Nde*I / *Hind*III restriction digest of vector and insert, followed by ligation yielding pET24a_scSRP^{219}2.

An N-terminal truncated version of FtsY with a Q345C mutation and an N-terminal penta-His-tag (FtsY^{219}Q345C) was PCR amplified and subcloned from a plasmid encoding the mutant FtsY Q345C (2) into a pET24a vector yielding pET24a_ FtsY^{219}Q345C.

Preparation of RNC^{Lep50} Complexes

A plasmid encoding the first 50 amino acids of the leader peptidase precursor with an N-terminal triple StrepII-tag followed by a TEV cleavage site was obtained from Genscript. This

Lep50-construct was subcloned into pUC19 yielding pUC19StrepLep50. The resulting plasmid was digested with *Hin*dIII, *in vitro* transcribed and translated using membrane-free cell extract (3). Sucrose gradient centrifugation and affinity purification were carried out as described (3) with the exception that all buffers contained 500 µg/ml chloramphenicol to stabilize the RNCs. After the final centrifugation step to concentrate the RNC^{Lep50} complexes, they were dissolved in buffer A (50 mM Hepes-KOH, 100 mM KOAc, 8 mM $Mg(OAc)_2$, pH 7.5, 500 µg/ml chloramphenicol).

GTPase Measurements

GTPase assays were carried out at 25°C in assay buffer [50 mM KHEPES, pH 7.5, 150 mM KOAc, 10 mM $Mg(OAc)_2$, 2 mM dithiothreitol (DTT), 0.5 µg/µL chloramphenicol and 0.01% Nikkol]. Hydrolysis of GTP was followed and analyzed by thin layer chromatography as described (4). GTPase reactions contain 50-100 nM wild-type or mutant scSRP construct, a two-fold excess of 4.5S RNA, and 100 µM GTP doped with γ-^{32}P-GTP (MP Biomedicals, Solon, OH).

Fluorescence Measurements

Fluorescence measurements were carried out at 25 °C on a FluoroLog-3-22 spectrofluorometer (Jobin-Yvon) in assay buffer. Where applicable, the buffer also contained 100-200 µM GMPPNP to induce formation of the closed complex. FRET between donor (DACM) and acceptor (BODIPY-FL)-labeled SRP(C153) and FtsY(C345) was measured using an excitation wavelength of 360 nm. Reactions contained 50–100 nM SRP, saturating concentrations of RNC^{Lep50} (100-200 nM), and saturating FtsY (1600 nM for closed complex, 500 nM for early complex) where applicable.

Nano-gold Labeling of scSRP ^{219}

Purified $scSRP^{219}2$ containing an N-terminal His-tag was incubated with a 5-fold molar excess of 1.8 nm Ni-NTA-Nanogold (Nanoprobes, INC) for 1h at 4C in binding buffer (50 mM Hepes pH 7.5, 100 mM KOAc, 8 mM MgOAc2). Excess of unbound Nanogold was removed

from the sample by purification of the labelled scSRP^{219} via its C-terminal StrepII tag followed by concentration and buffer exchange to buffer A using an Amicon Ultra-4 centrifugal filter unit (MWCO 50 kDA, Millipore). RNC^{Lep50}-scSRP^{219}-GMPPCP complexes were prepared for cryo-EM as described above with a 10-fold excess of scSRP^{219} and 1mM GMPPCP. Cryo-EM data were collected on a Tecnai G2 Polara (FEI) operating at 100 kV and a specimen level magnification of 76,000x with a Gatan 4k x 4k CCD camera in a defocus range between −0.7 µm and −5.7 µm with an initial pixel size of 1.86 Å on the object scale.

The contrast transfer function (CTF) was determined and corrected with bctf (Bsoft package). 19,699 particles were selected semi-automatically from 207 CCD frames using e2boxer (EMAN2). For alignments, the particles were re-sampled to 3.72 Å/pixel, inverted and low-pass-filtered to 12 Å. The particles were aligned using a low pass filtered vacant ribosome as initial reference (EMDB ID: 1045) in SPIDER (5). Classification according to presence of scSRP^{219}2 at the ribosomal tunnel exit in SPIDER resulted in a total number of 6,402 particles representing RNC^{Lep50}-scSRP^{219}2-GMPPCP. This particle pool was further classified into 100 classes by multivariate statistical analysis (MSA) and classification in IMAGIC-5 (6). Classes showing orientations of the RNC^{Lep50}-scSRP^{219}2-GMPPCP complexes where scSRP^{219} is clearly visible were identified by projection matching to a ribosomal map using SPIDER (5) and the corresponding 368 particles were submitted to a second round of MSA and classification into 20 classes using IMAGIC. Nine of these classes were identified to contain clearly visible SRP density using SPIDER. The calculated alignment and classification parameters were used to identify and align the corresponding not-inverted full-sized particles. The position of the nano-gold was marked manually in each aligned particle using boxer (EMAN, (7)) and plotted for the three most populated classes in which scSRP^{219}2 is distinguishable.

SI FIGURES

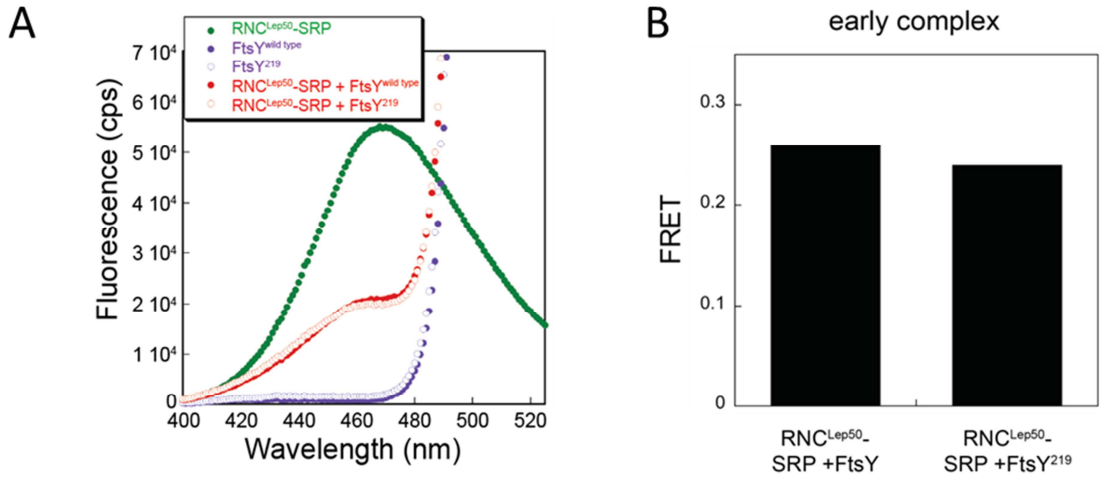

Figure S1: FRET measurements of the *early* complexes.

(A) Fluorescence emission spectra of DACM-labeled RNC^{Lep50} -SRP, BODIPY-FL labeled FtsY or $FtsY^{219}$, and the RNC^{Lep50} -SRP-FtsY (wild type) and RNC^{Lep50} -SRP-$FtsY^{219}$ complexes in the presence of GMPPNP. **(B)** FRET values calculated based on the fluorescence emission spectra of the fluorescence dye-labeled RNC^{Lep50}-SRP-FtsY (wild type) and RNC^{Lep50}-SRP-$FtsY^{219}$ complexes in the absence of nucleotide. Both targeting complexes are adopting the *early* state. The labeling and measurements were done exactly the same way as described for the *closed* complex.

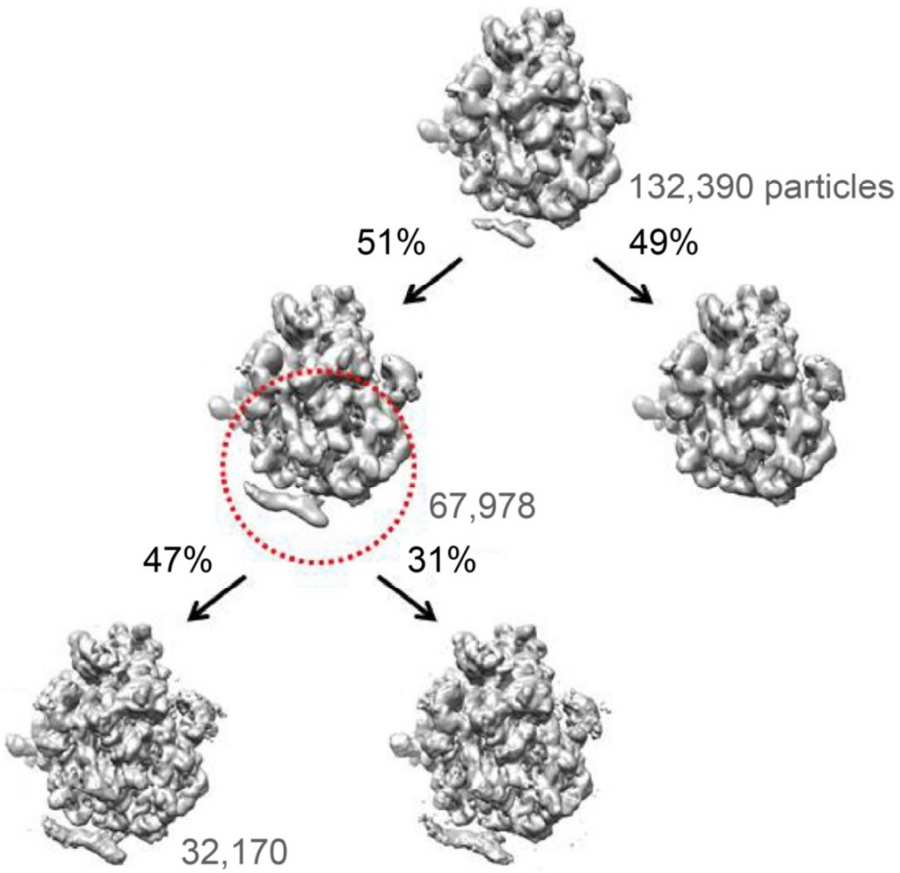

Figure S2: Computational sorting of the RNC^{Lep50}-scSRP^{219}-GMPPCP data set.

An initial map was generated using all 132,390 particles of the data set (first row). The particles were then separated according to whether they align better to the initial map, or to a modified map in which the density corresponding to scSRP^{219} was deleted in Chimera (8). This led to a SRP-containing pool and a vacant pool (second row). Next, a spherical mask centred near the ribosomal tunnel exit with a radius of 130 Å was applied to the SRP-containing pool for further un-supervised classification using Relion (9). The edge of the mask is indicated by red dots. In this round, ~22% particles were discarded based on low correlation coefficient. Using this sorting approach, we observed two similar ribosome-scSRP^{219} complex structures containing 32,170 particles and 20,203 particles, and two additional volumes with low particle numbers representing low-quality particles in the pool. The pool containing 32,170 particles (24.3% of the total data set) displayed a SRP density that was better defined compared to the second pool, and was therefore used for the final refinement.

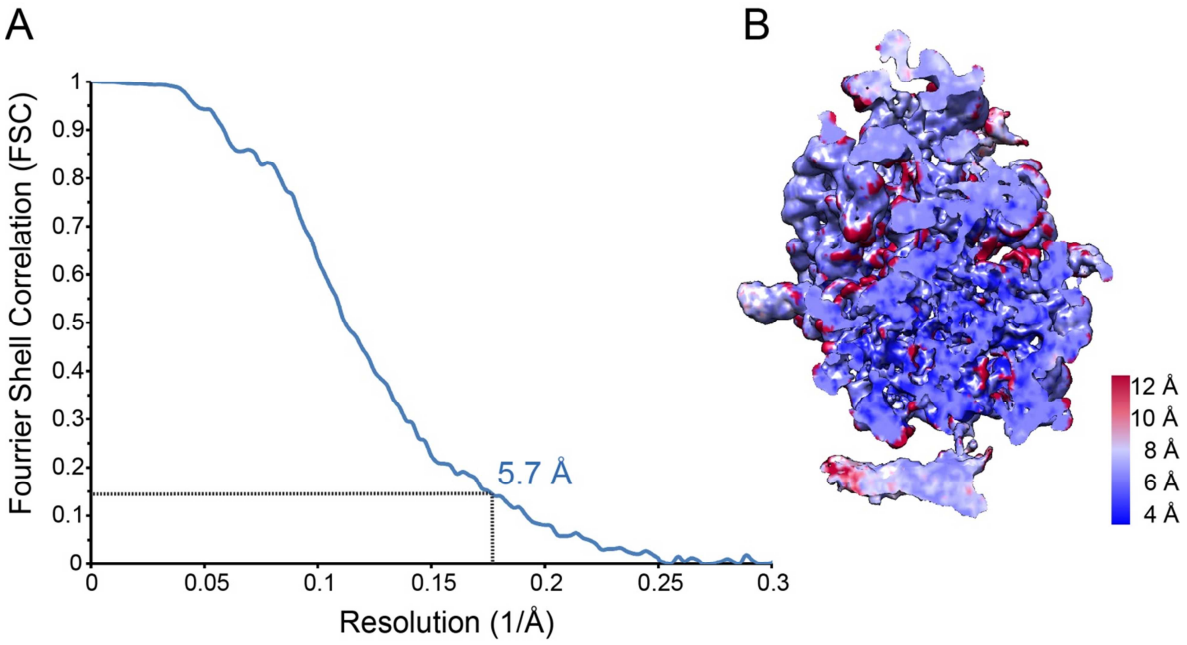

Figure S3: Resolution of the cryo-EM reconstruction of the *closed* RNC-SRP-FtsY complex. (A) Fourier Shell Correlation (FSC) curve of the cryo-EM reconstruction of the *closed* targeting complex, obtained by refining a separate model for two independent halves of the data in RELION (9). The resolution estimate is 5.7 Å according to the FSC = 0.143 criterion (10) and 9.0 Å according to the FSC = 0.5 criterion. **(B)** Local resolution estimation of the cryo-EM reconstruction. The unfiltered, non-sharpened cryo-EM map is shown in a sliced view. The local resolution has been measured using the ResMap program (11). The map is colored based on the calculated local resolution from 4 Å (dark blue) to 12 Å (red).

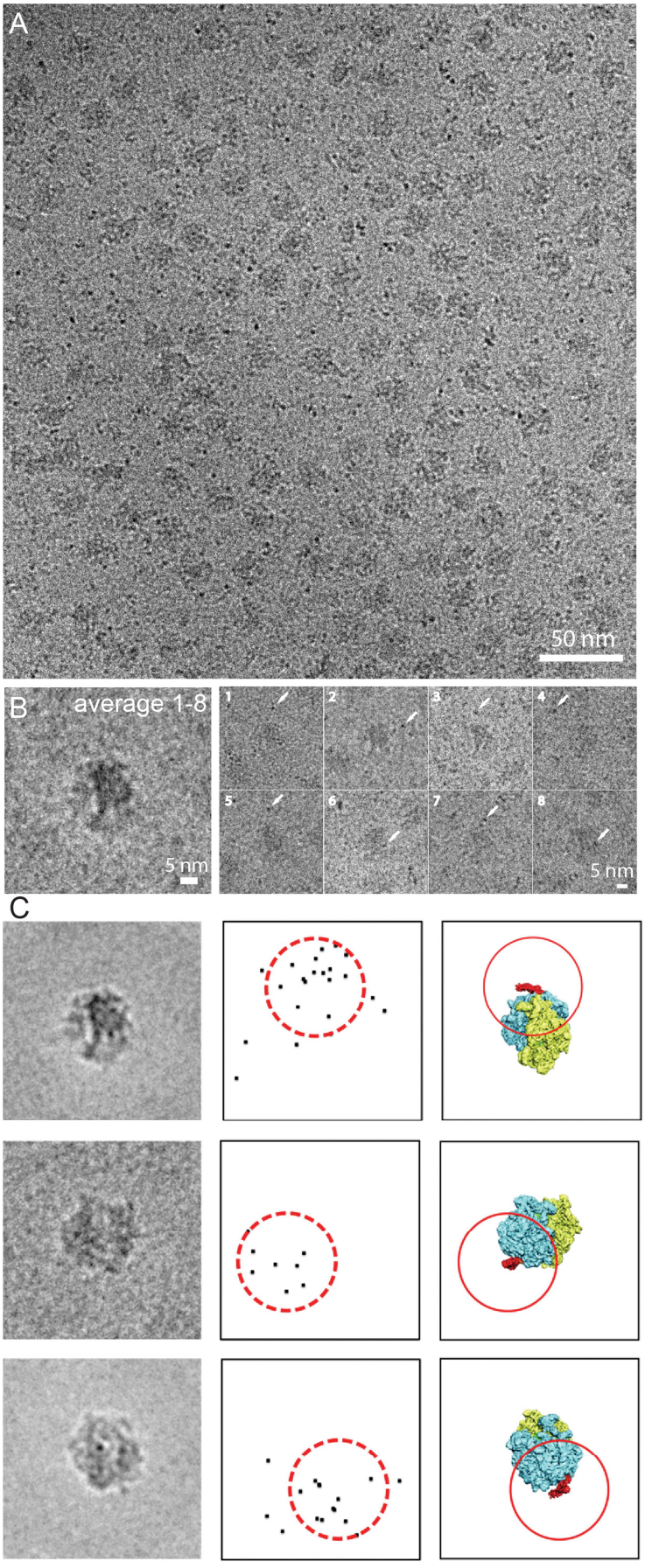
A
50 nm
B
average 1-8
5 nm
1
2
3
4
5
6
7
8
5 nm
C

Figure S4: Nano-gold-labeling of the FtsY-Ffh NG-domains and cryo-EM localization experiments. (A) A typical micrograph with RNC^{Lep50} and gold-labeled $scSRP^{219}2$ particles in the presence of GMPPCP. To shift the equilibrium towards complex formation, $scSRP^{219}2$ was added in ten-fold molar excess to ribosomes. **(B)** Eight individual particles used for localization of the FtsY-Ffh-NG domains and the average of these eight individual $scSRP^{219}2$-RNC particles calculated with SPIDER (AS R). Gold particles that were picked are indicated by a white arrow. Gold particles positioned at the edge of the box were not picked. A 50 nm scale bar and a 5 nm scale bar are shown for the micrograph and the particles, respectively. **(C)** 2D class averages of gold-labeled particles in three orientations in which SRP density can be identified (first column), plot of the position of the nano-gold in the individual images that were used to generate the 2D class averages (column 2) and surface view of the same orientation as the 2D class average (column 3). The red circle (dashed line in the plots of the gold position and solid line in the surface representation) indicates the theoretical volume in which the nano-gold could be theoretically found in the *closed* complex assuming flexible Ffh-FtsY NG-domains.

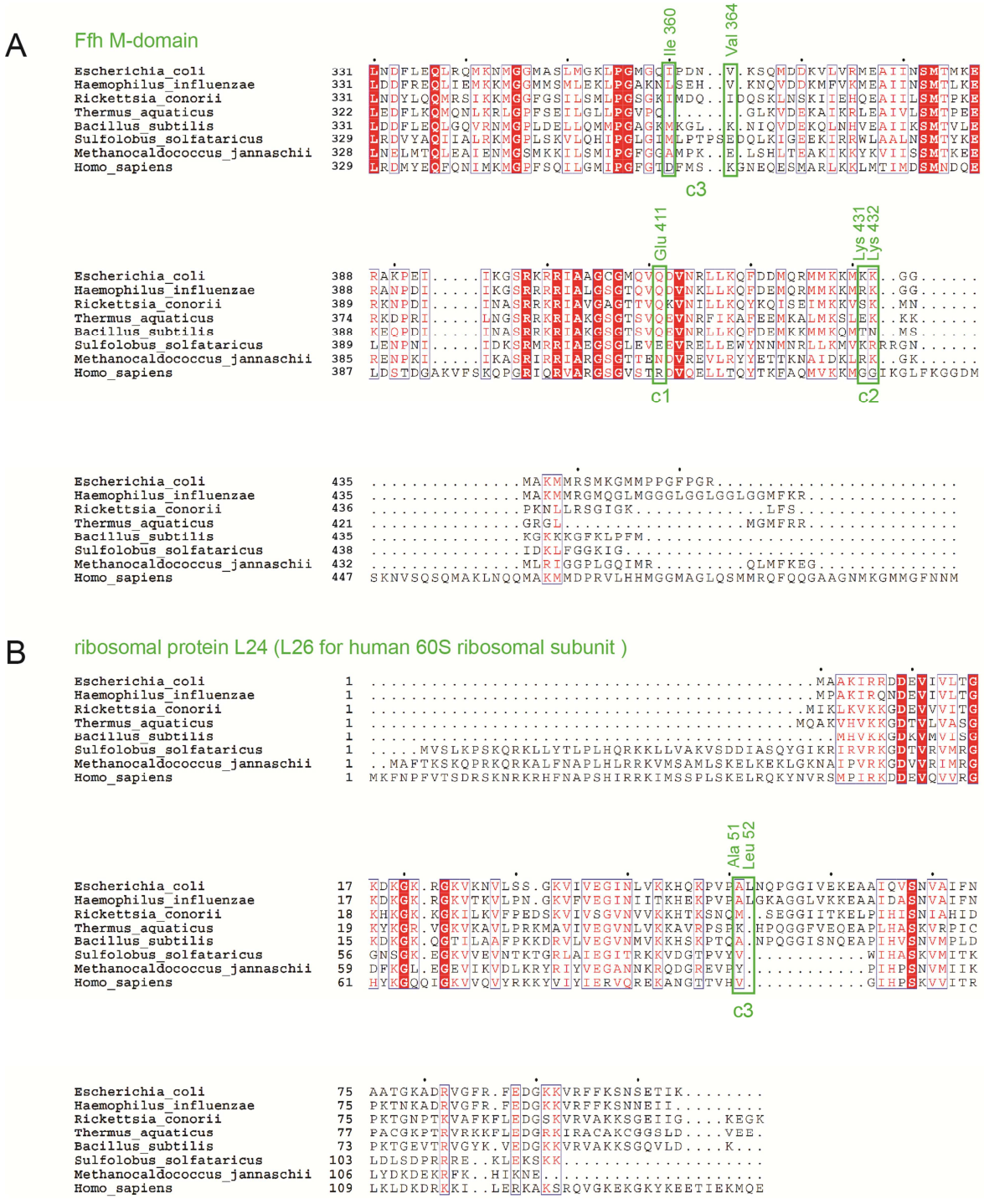

Figure S5: Conservation of M-domain residues involved in ribosomal contacts in the *closed* state.

(A) Alignment of M-domain sequences from Gram-negative and Gram-positive (*B. subtilis*) bacteria, archaea (*S. solfataricus* and *M. jannaschii*), and human. SRP crystal structures have been reported for *E. coli*, *T. aquaticus*, *S. solfataricus*, *M. jannaschii* and human. **(B)** Alignment of ribosomal protein L24 (L26 in human) sequences from the same species as in panel A. Conservation is indicated by color intensity. Among bacteria significant conservation is observed in the residues involved in ribosomal contacts (c1-c3) which are marked in green.

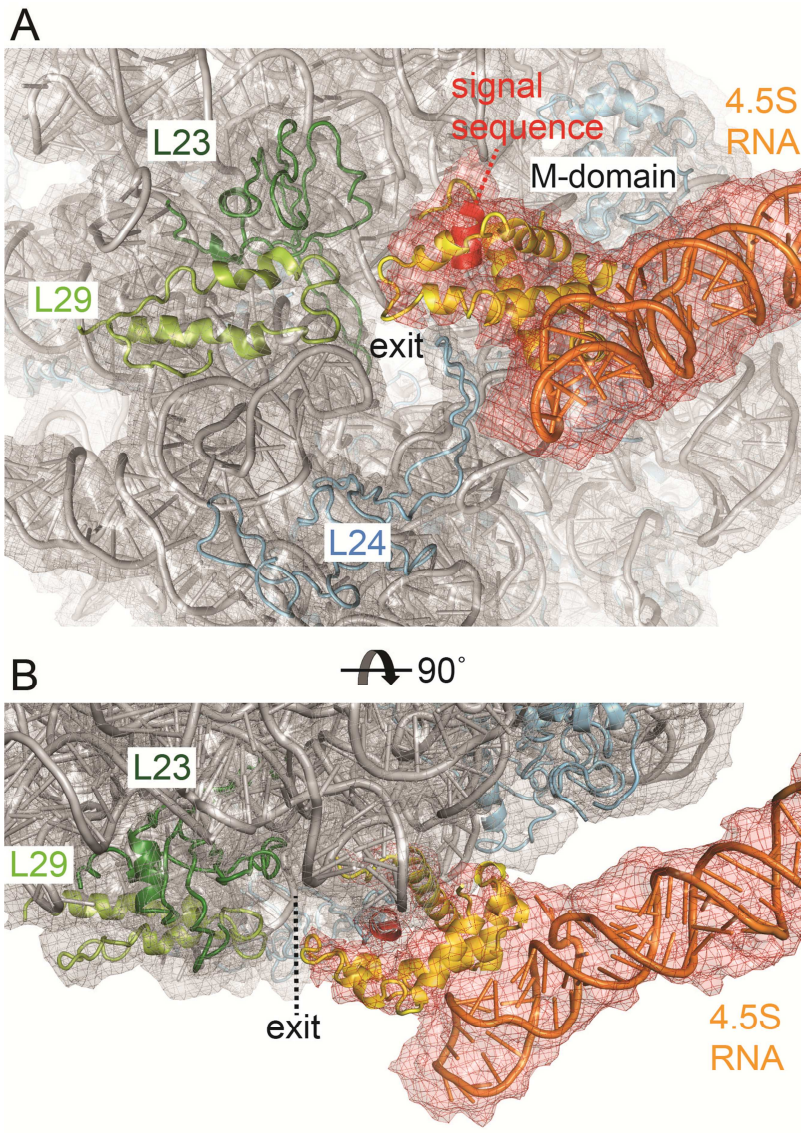

Figure S6: Ribosomal proteins L23 and L29 are accessible for translocon binding in the *closed* state. The structure and the quasi-atomic model are shown **(A)** in a view into the exit of the ribosomal tunnel and **(B)** in a side view. Density corresponding to the ribosome is depicted in transparent grey, density corresponding to the SRP in red. The SRP RNA is colored orange, the M-domain yellow and the signal sequence red. The ribosomal RNA is shown in grey, ribosomal proteins in cyan, L29 in green-yellow and L23 in forest. The position of the exit is marked.

SI REFERENCES:

1. Estrozi LF, Boehringer D, Shan SO, Ban N, Schaffitzel C (2011) Structure of the *E. coli* co-translational targeting complex in the stable *early* conformation. *Nat Struct Mol Biol* 18:88-90.

2. Zhang X, Kung S, Shan SO (2008) Demonstration of a multistep mechanism for assembly of the SRP x SRP receptor complex: implications for the catalytic role of SRP RNA. *J Mol Biol* 381(3):581-593.

3. Schaffitzel C, Ban N (2007) Generation of ribosome nascent chain complexes for structural and functional studies. *J Struct Biol* 158(3):463-471.

4. Peluso P, Shan SO, Nock S, Herschlag D, Walter P (2001) Role of SRP RNA in the GTPase cycles of Ffh and FtsY. *Biochemistry* 40(50):15224-15233.

5. Shaikh TR, *et al.* (2008) SPIDER image processing for single-particle reconstruction of biological macromolecules from electron micrographs. *Nat Protoc* 3(12):1941-1974.

6. van Heel M, Harauz G, Orlova EV, Schmidt R, Schatz M (1996) A new generation of the IMAGIC image processing system. *J Struct Biol.* 116(116):17-24.

7. Tang G, *et al.* (2007) EMAN2: an extensible image processing suite for electron microscopy. *J Struct Biol* 157(1):38-46.

8. Pettersen EF, *et al.* (2004) UCSF Chimera--a visualization system for exploratory research and analysis. *J Comput Chem* 25(13):1605-1612.

9. Scheres SH (2012) RELION: implementation of a Bayesian approach to cryo-EM structure determination. *J Struct Biol* 180(3):519-530.

10. Rosenthal PB, Henderson R (2003) Optimal Determination of Particle Orientation, Absolute Hand, and Contrast Loss in Single-particle Electron Cryomicroscopy. *J Mol Biol* 333(4):721-745.

11. Kucukelbir A, Sigworth FJ, Tagare HD (2014) Quantifying the local resolution of cryo-EM density maps. *Nature Methods* 11(1):63-65.